Ionization Behavior, Stoichiometry of Association, and Accessibility of Functional Groups in the Active Layers of Reverse Osmosis and Nanofiltration Membranes

ARTICLE *in* ENVIRONMENTAL SCIENCE & TECHNOLOGY · SEPTEMBER 2010

Impact Factor: 5.33 · DOI: 10.1021/es100891r · Source: PubMed

Environ. Sci. Technol. **2010,** *44,* 6808–6814

Ionization Behavior, Stoichiometry of Association, and Accessibility of Functional Groups in the Active Layers of Reverse Osmosis and Nanofiltration Membranes

ORLANDO CORONELL,[†,||] MARI I. GONZÁLEZ,[‡,||] BENITO J. MARIÑAS,[*,‡,||] AND DAVID G. CAHILL[§,||]

Department of Environmental Sciences and Engineering, Gillings School of Global Public Health, University of North Carolina at Chapel Hill, Chapel Hill, North Carolina 27599, and Department of Civil and Environmental Engineering, Department of Materials Science and Engineering, and Science and Technology Center of Advanced Materials for the Purification of Water with Systems, University of Illinois at Urbana−Champaign, Urbana, Illinois 61801

Received March 19, 2010. Revised manuscript received July 14, 2010. Accepted July 21, 2010.

We characterized the fully aromatic polyamide (PA) active layers of six commercial reverse osmosis (RO) and nanofiltration (NF) membranes and found that in contrast to their similar elemental composition, total concentration of functional groups, and degree of polymerization, the ionization behavior and spatial distribution of carboxylic (R-COOH) groups within the active layers can be significantly different. We also studied the steric effects experienced by barium ion (Ba^{2+}) in the active layers by determining the fraction of carboxylate ($R\text{-}COO^-$) groups accessible to Ba^{2+}; such fraction, referred to as the accessibility ratio (AR), was found to vary within the range AR = 0.40−0.81, and to be generally independent of external solution pH. Additionally, we studied an NF membrane with a sulfonated polyethersulfone (SPES) active layer, and found that the concentration of sulfonate ($R\text{-}SO_3^-$) groups in the active layer was 1.67 M, independent of external solution pH and approximately three times higher than the maximum concentration ($\approx 0.45 \pm 0.25$ M) of $R\text{-}COO^-$ groups in PA active layers. The $R\text{-}SO_3^-$ groups were found to be highly accessible to Ba^{2+} (AR $= 0.95 \pm 0.01$).

Introduction

Reverse osmosis (RO) and nanofiltration (NF) membranes are increasingly attractive technologies for water treatment because they provide effective control of a broad range of contaminants. The structure of most RO/NF membranes consists of a top ultrathin polyamide (PA) active layer (∼50−200 nm), an intermediate polysulfone support, and a polyester backing (*1*). Membrane performance is mostly controlled by the interaction of water and contaminants with the active layer (*1*−*5*), and therefore understanding the relation between active layer physicochemical properties and the permeation of water and solutes would enable the systematic optimization of RO/NF membranes for applications involving specific contaminants.

Unfortunately, despite decades of research, it is currently not possible to directly relate the physicochemical properties of active layers to RO/NF membrane performance, partly because of the limited amount of quantitative data available about key active layer properties and interactions with water and contaminants. While experimental studies of the surface of active layers are relatively abundant (*4, 6*−*8*), studies of their inner region are more scarce (*9*) due to limitations associated with the nanometer-scale resolution required to characterize these ultrathin (∼100 nm) films. Among the properties in the inner region that have been experimentally studied (*9*), only a few (e.g., pore size distribution (*10*), elemental composition (*11*)) have been quantified in several commercial RO/NF membranes. As a result, there is a need to gather more data on the properties of the inner region of active layers, and their interaction with contaminants, to better understand what differentiates one RO/NF membrane from another.

Active layer properties that affect membrane performance include the concentration of ionizable functional groups and their interactions with ionic contaminants. Ionizable functional groups affect water and solute permeation not only because they produce pH-dependent charges in the active layer (*1, 5*), but also because they are directly related to the active layer structure (*12, 13*). Most notably, in PA active layers ionizable functional groups are related to the degree of polymer cross-linking (*1, 12*) because each carboxylic ($R\text{-}COOH/R\text{-}COO^-$) and amine ($R\text{-}NH_3^+/R\text{-}NH_2$) group in the PA structure corresponds to an amide link not formed during the PA polymerization reaction (*1*).

Accordingly, the objective of this study is to quantify various properties related to ionizable functional groups in the active layers of five RO/NF membranes with fully aromatic PA active layers, and one NF membrane with a sulfonated polyethersulfone (SPES) active layer. Properties studied include (i) concentration of functional groups and their ionization behavior as a function of pH; (ii) degree of polymer cross-linking; (iii) stoichiometry of association between negative functional groups and Ba^{2+} ion; and (iv) steric effects experienced by Ba^{2+}. The findings of this study advance the quantitative understanding of physicochemical properties of active layers, and provide valuable data that form the basis for subsequent research on how these properties control transport in RO/NF membranes.

Materials and Methods

Membranes. Six RO/NF membranes were studied: LF10 RO and NTR-7450 NF (Nitto Denko, Japan), ESPA3 RO and ESNA NF (Hydranautics, Oceanside, CA), NF90 NF (Dow Liquid Separation, Midland, MI), and TFC-S NF (Koch Membrane Systems, Wilmington, MA). NTR-7450 has a sulfonated polyethersulfone (SPES) active layer with negative sulfonate ($R\text{-}SO_3^-$) groups (*1, 11*); all other membranes have fully aromatic polyamide (PA) active layers (see spectroscopic analyses in Figure S1 of Supporting Information (SI)) with negatively ionizable carboxylic ($R\text{-}COOH/R\text{-}COO^-$) and positively ionizable amine ($R\text{-}NH_3^+/R\text{-}NH_2$) groups (*1, 12*).

* Corresponding author tel: +1-217-333-6961; fax: +1-217-333-6968; e-mail: marinas@illinois.edu.
† University of North Carolina at Chapel Hill.
‡ Department of Civil and Environmental Engineering, University of Illinois at Urbana−Champaign.
§ Department of Materials Science and Engineering, University of Illinois at Urbana−Champaign.
|| Science and Technology Center of Advanced Materials for the Purification of Water with Systems, University of Illinois at Urbana−Champaign.

10.1021/es100891r

Published on Web 08/11/2010

Even though semiaromatic PA is a common material in NF membranes, using only fully aromatic membranes enabled us to compare RO and NF membranes having the same basic structure. All experiments were performed at room temperature (20−22 °C) with 2.5 × 5.0-cm^2 coupons rinsed with and stored in nanopure water. In general, three samples were prepared for each condition tested.

Quantification of Ionized Functional Groups. Concentrations of ionized functional groups in active layers were obtained as a function of pH using experimental methods developed in our previous studies of the FT30 RO membrane (*12, 14*). Negative functional groups in active layers were quantified in the pH range 3.4−10.5 by first saturating them with silver ions (Ag^+), and subsequently quantifying the concentration of Ag^+ associated with the ionized groups using Rutherford backscattering spectrometry (RBS). We assume that the measured Ag^+ concentration in the active layer is equivalent to the concentration of negative functional groups. A representative RBS spectrum for a sample of LF10 RO membrane probed with Ag^+ is shown in Figure S2 of SI. Positive functional groups were quantified in the pH range 3.8−7.4 using tungstate (WO_4^{2-}) as ion probe. We assume that the concentration of WO_4^{2-} in the active layer is approximately equal to the concentration of positive sites. Additional details about experimental procedures can be found in refs *12 and 14*.

Stoichiometry of Association between Negative Functional Groups and Ba^{2+}. Ba^{2+} ion was chosen as ion probe due to its following properties (*14*): (i) divalence—to study stoichiometry of association; (ii) ionic radius larger than the radius of the smallest pores in PA active layers—to study steric effects (see below); and (iii) relatively large atomic mass—to ensure accurate quantification by RBS at the concentrations that functional groups are present in active layers. In brief, we first saturated with Ag^+ the negative functional groups in the active layers. Next, we used Ba^{2+} ions to displace Ag^+ ions. The concentrations of Ag^+ and Ba^{2+} in the active layer before and after ion displacement were quantified by RBS with the drop in Ag^+ concentration ($\Delta[Ag^+]$) providing the concentration of sites neutralized by Ba^{2+}. The average stoichiometry of association at a given pH between sites neutralized by Ba^{2+} and the Ba^{2+} ions neutralizing those sites (i.e., the neutralization number NN), defined as (*14*)

$$\mathrm{NN} = \frac{\text{Concentration of negative charges neutralized by } Ba^{2+}}{\text{Concentration of } Ba^{2+} \text{ neutralizing negative charges}} \quad (1)$$

was calculated as $\mathrm{NN} = \Delta[Ag^+]/[Ba^{2+}]$, where $[Ba^{2+}]$ is the Ba^{2+} concentration in the active layer after ion displacement. NN was studied as a function of the concentration of neutralized sites by performing Ag^+−Ba^{2+} displacement experiments in the pH range 6.0−10.3. Experimental details about Ag^+−Ba^{2+} displacement tests can be found elsewhere (*14*).

Ion Probing with Ba^{2+} and K^+. Using the ion-probing/RBS procedure (see above and ref *14*), the concentration of Ba^{2+} that associates with negative functional groups in the active layers of the membranes studied was characterized in the pH range 3.5−10.3. Additionally, the concentration of K^+ that associates with R-SO_3^- groups in the active layer of the NTR-7450 membrane was quantified in the pH range 5.3−8.8.

Ion-Probe Solutions. Solutions were prepared with nanopure water and ACS grade chemicals with 99%+ purity. Barium chloride dihydrate ($BaCl_2 \cdot 2H_2O$) (Fisher Scientific, Hampton, NH), and barium nitrate ($Ba(NO_3)_2$), silver nitrate ($AgNO_3$) and sodium tungstate (Na_2WO_4) (Sigma-Aldrich, St. Louis, MO) were used as sources of Ba^{2+}, Ag^+, and WO_4^{2-}. The concentrations of barium (10^{-6}−0.32 M), silver (10^{-6}−10^{-3} M) and tungstate (10^{-6}−10^{-3} M) in solution were always below their solubility limits (*15*). NaOH and HCl were used for pH adjustment, except in the case of experiments involving silver for which NaOH and HNO_3 were used to avoid AgCl precipitation. Solutions containing silver were prepared and used under dim red light to avoid photoreactivity.

RBS Analyses. Details on RBS theory and analysis and RBS use to quantify the elemental composition of active layers (*6, 11, 16*) and the concentration of heavy ions in them (*14, 16*) can be found elsewhere. RBS is a thin-film analysis technique in which a high energy ion beam is directed to the test sample, and the energy and number of ions backscattered at a certain angle are recorded. The resulting spectrum is analyzed to obtain the sample elemental composition as a function of depth. In this study, we used a circular, 3-mm, 2-MeV He^+ beam generated with a Van de Graaff accelerator. For each membrane sample, data were collected by scanning the beam over ~8 cm^2 of the surface keeping the He^+ ion fluence below the threshold of 3×10^{14} He^+/cm^2 above which the integrity of the membrane is compromised (*17*). The incident, exit, and scattering angles of the He^+ beam were 22.5°, 52.5°, and 150°, respectively. The software SIMNRA (*18*) was used for data analysis.

Results and Discussion

Elemental Composition and Thickness of Active Layers. Table 1 shows the RBS results for the elemental composition and thickness of the active layers studied including results previously reported for the FT30 RO membrane (*12, 14*). For any given sample, active layer thickness was modeled as a Gamma distribution of thicknesses described by a corresponding average (δ) and standard deviation (σ) (*11*). RBS spectra and simulations for untreated membranes are presented in Figure S4 of SI. The analysis of the onset energy of the nitrogen peak in the RBS spectra of the LF10 RO membrane (see ref *12* for analysis using the FT30 membrane) revealed the existence of a coating layer on top of the active layer; the coat was $\delta \pm \sigma = 58 \pm 33$-nm thick with approximate composition $C_{0.28}O_{0.12}H_{0.60}Cl_{0.001}$, similar to the 25 ± 35-nm thick coat ($C_{0.32}O_{0.12}H_{0.56}$) reported (*12*) for the FT30 RO membrane. The relatively high O:C ratios in the coatings are consistent with the use of cross-linked polyvinyl alcohol as coating material (*1, 19*). Analyses of the RBS spectra of all other membranes showed that all NF membranes lacked coatings, consistent with studies (*20, 21*) by attenuated total reflectance Fourier transform infrared (ATR-FTIR) spectroscopy in which only four RO membranes, out of nine RO and four NF membranes analyzed, had coatings. We hypothesize that despite the benefits provided by coat layers (e.g., increased fouling resistance (*1, 19*)), they are not used in NF membranes because coat layers also reduce clean water flux (*19*), therefore decreasing the maximum achievable water productivity.

Table 1 also shows no major differences between RO and NF membranes with respect to the elemental compositions of uncoated PA active layers; oxygen contents in coated active layers, however, are distinctly higher than in uncoated ones, which possibly is an artifact resulting from RBS being unable to accurately differentiate the oxygen in the PA active layer from that in the coat layer. We did not test this hypothesis experimentally as it is not possible to perform RBS analysis in the absence of the coats.

Consistent with the relatively high roughness reported (*11, 13, 21*) for PA active layers, Table 1 shows that the thickness of PA active layers is markedly nonuniform with thickness standard deviations of 39−61% of the corresponding average thicknesses. Table 1 also suggests that fully aromatic PA RO active layers are typically thicker than their NF counterparts with average thicknesses of 111 and 90 nm

TABLE 1. Summary of Results for the RBS and Ion-Probing/RBS Analyses of the Active Layers of the RO/NF Membranes Studied (Uncertainties Represent Standard Error)

membrane	FT30[a,b] RO	LF10[b] RO	ESPA3 RO	TFC-S NF	ESNA NF	NF90 NF	NTR-7450 NF
C	0.48	0.48	0.49	0.49	0.49	0.50	0.47
O	0.12	0.13	0.09	0.09	0.09	0.08	0.15
N	0.07	0.06	0.08	0.08	0.09	0.08	–
S	–	–	–	–	–	–	0.04
Cl	0.00	0.008	0.008	0.006	0.012	0.002	–
H[c]	0.32	0.32	0.33	0.33	0.33	0.33	0.34
O:N ratio	1.77	2.34	1.12	1.25	1.00	0.96	–
$\delta \pm \sigma$[d] (nm)	120 ± 47	116 ± 55	98 ± 57	72 ± 41	87 ± 53	111 ± 56	142 ± 65
$C_{T,\text{R-COOH}}$ (M)	0.54 ± 0.02	0.50 ± 0.02	0.64 ± 0.01	0.54 ± 0.01	0.51 ± 0.01	0.24 ± 0.02	1.67 ± 0.02[g]
$pK_{a,1}$	5.39 ± 0.23	5.23 ± 0.16	3.91 ± 1.06	5.38 ± 0.11	5.42 ± 0.13	5.72 ± 0.06	–
$pK_{a,2}$	9.03 ± 0.08	8.46 ± 0.17	5.86 ± 0.10	8.66 ± 0.06	8.67 ± 0.11	9.87 ± 0.23	–
w_1	0.22 ± 0.03	0.49 ± 0.05	0.08 ± 0.07	0.33 ± 0.02	0.45 ± 0.03	0.60 ± 0.04	–
w_2	0.78 ± 0.03	0.51 ± 0.05	0.92 ± 0.07	0.67 ± 0.02	0.55 ± 0.03	0.40 ± 0.04	–
$C_{T,\text{R-NH2}}$ (M)	0.04 ± 0.01	0.01 ± <0.005	0.01 ± <0.005	0.02 ± <0.005	0.01 ± <0.005	0.08 ± 0.04	–
$pK_{a,\text{R-NH3+}}$	4.62 ± 0.28	4.07 ± 0.09	3.68 ± 0.21	3.63[h]	3.63[h]	3.63 ± 0.35	–
$C_{T,\text{R-COOH}}/C_{T,\text{R-NH2}}$	0.08 ± 0.02	0.03 ± 0.002	0.01 ± 0.005	0.03 ± 0.004	0.03 ± 0.001	0.33 ± 0.18	0.00[i]
isoelectric point	4.5	4.1	3.3	3.4	3.5	4.3	–
DPC[e]	0.94 ± 0.07[j]	0.94 ± 0.06[j]	0.95 ± 0.07[j]	0.95 ± 0.07[j]	0.96 ± 0.07[j]	0.97 ± 0.07[j]	–
α[e] (M)	0.03 ± <0.01	0.17 ± 0.01	0.28 ± 0.02	0.14 ± 0.01	0.12 ± 0.02	NN = 1.98 ± 0.20[k]	NN = 1.96 ± 0.05[k]
AR[e]	0.40 ± 0.04	0.58 ± 0.03	0.62 ± 0.04	0.81 ± 0.03	0.44 ± 0.02	0.58 ± 0.03	0.95 ± 0.01
n[f]	0.64 ± 0.07	0.59 ± 0.04	0.66 ± 0.11	0.68 ± 0.04	0.73 ± 0.02	0.84 ± 0.07	$k = 2.00$[l]
x[f]	0.34 ± 0.07	0.40 ± 0.04	0.34 ± 0.11	0.31 ± 0.04	0.26 ± 0.02	0.12 ± 0.07	$l = 1.08$[l]
y[f]	0.03 ± 0.01	0.01 ± 0.001	0.005 ± 0.002	0.01 ± 0.001	0.01 ± 0.001	0.04 ± 0.02	$i = 0.75$[l]

[a] For consistency with the RBS data analysis performed for the other membranes in Table 1, the RBS data previously reported in refs *12 and 14* for the FT30 RO membrane were reanalyzed taking into account the recently obtained density (1.24 g/cm^3) of its polyamide (PA) active layer (*31*) and other minor improvements to RBS simulation. The results presented in Table 1 are only slightly different from those reported before (*12, 14*), and do not affect any of the conclusions reported in previous publications (*12, 14*). [b] The PA active layers of the FT30 RO and LF10 RO membranes were found to have active layer coatings of approximate composition and thickness $C_{0.32}O_{0.12}H_{0.56}$ and 25 ± 35 nm, and $C_{0.28}O_{0.12}H_{0.60}Cl_{0.001}$ and 58 ± 33 nm, respectively. [c] Because RBS spectra do not have a hydrogen Rutherford scattering signal, but are affected by the stopping power of the hydrogen content, analysis of RBS data for polymers requires the input of their H:C ratio (*11*). The ratio assumed for the sulfonated polyethersulfone (SPES) active layer of the NTR-7450 NF membrane was H:C = 0.69 (*29*) (see Figure S3 of SI), and that for fully aromatic PA active layers was H:C = 0.67 (*11*). [d] Active layer thickness was modeled as a Gamma distribution of thicknesses with δ and σ as the average and standard deviation values, respectively. For the calculation of active layer thickness, the density of the active layer is needed (*14, 31*); we used 1.24 g/cm^3 (*31*) and 1.37 g/cm^3 (*32*) for PA and SPES, respectively. For coat layers, we used the density of amorphous polyvinyl alcohol (PVA) (1.26 g/cm^3) (*33*) consistent with reports of the use of PVA as coating material (*1, 19*). [e] DPC (degree of polymer cross-linking), AR (accessibility ratio), and α parameter in eqs 4, 5, and 6, respectively. [f] Fractions of polymer repeating units that are fully cross-linked (n), contain a carboxylic group (x), and contain an amine group (y). Uncertainties are mainly determined by the error-to-value ratio of the fitted total concentration of amine groups which is high due to the inability to obtain WO_4^{2-}-probing data below pH ≈ 3.8. [g] Concentration of sulfonate groups ($C_{T,\text{R-SO3-}}$) in the SPES active layer. [h] Given the limited number of data points for the probing of R-NH_3^+ with WO_4^{2-} in the TFC-S NF and ESNA NF membranes, for these two membranes we only fitted $C_{T,\text{R-NH2}}$ using $pK_{a,\text{R-NH3+}} = 3.63$ obtained through the fitting of the data of the third PA nanofiltration membrane, NF90. [i] The concentration of positive sites in the SPES active layer was quantified in the pH range 4.00−5.67 and was found to be zero. [j] Uncertainty was calculated assuming a 5% error in nitrogen content. [k] For the NF90 NF membrane, α = 0.00 ± <0.01, and as a result, we report the experimental NN. For the NTR-7450 NF membrane, the α parameter lacks practical physical meaning because the concentration of ionized sulfonate groups was constant across the pH range studied. Accordingly, we report the experimental NN. [l] Fractions of repeating units k, l, and i making up the composition of the SPES active layer as defined in Figure S3 of SI.

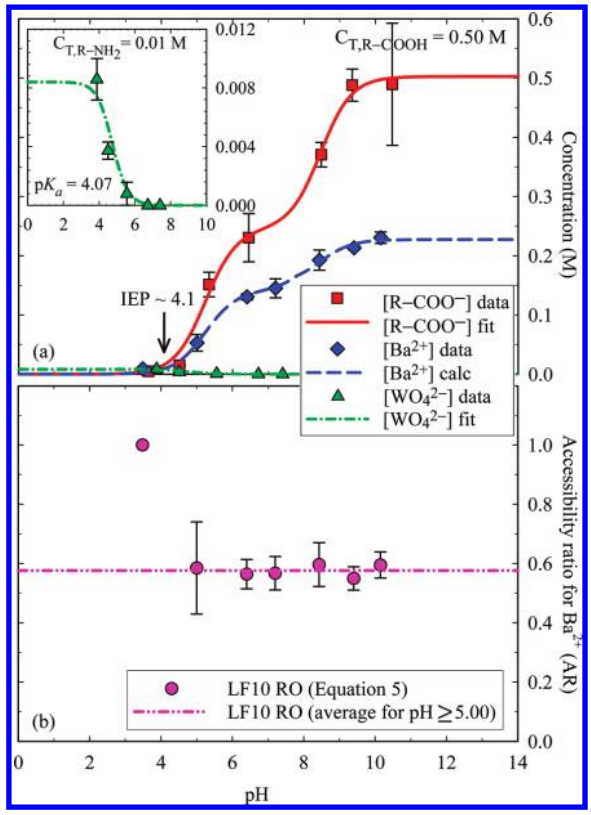

FIGURE 1. (a) Concentrations of R-COO$^-$ ([R-COO$^-$]) and R-NH$_3^+$ ([R-NH$_3^+$]) groups in the polyamide active layer of the LF10 RO membrane measured using Ag$^+$ and WO$_4^{2-}$, respectively, as ion probes. The concentration of Ba^{2+} ([Ba^{2+}]) that associates with accessible R-COO$^-$ groups in the active layer is also shown. Symbols represent experimental data. Error bars indicate standard deviation. The (red) continuous and (green) dot-dash lines are the fit lines of [R-COO$^-$] with eq 2 and [R-NH$_3^+$] with eq 3, respectively. The (blue) dashed line is the calculated [Ba^{2+}] using eqs 5 and 6 with α and AR values from Table 1. (b) Accessibility ratio for Ba^{2+} ion (AR) in the active layer of the LF10 RO membrane. Circles correspond to AR values calculated by solving eqs 5 and 6 using the [R-COO$^-$] and [Ba^{2+}] information from (a), and the α parameter from Table 1. At the lowest experimental pH of 3.48, we found that AR $\approx$ 1. Error bars indicate standard error. The dash-dot-dot line is the average AR = 0.58 $\pm$ 0.03 for the pH range of 5.00−10.15.

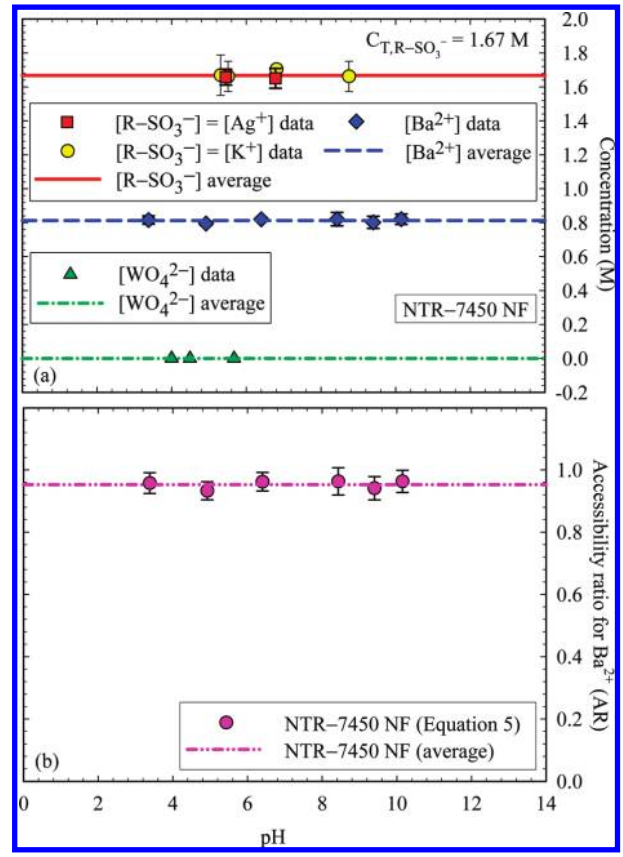

FIGURE 2. (a) Concentration of sulfonate groups ([R-SO$_3^-$]) in the sulfonated polyethersulfone (SPES) active layer of the NTR-7450 NF membrane measured using Ag$^+$ (squares) and K$^+$ (circles) as ion probes. The absence of positive functional groups was verified using WO$_4^{2-}$ (triangles) as ion probe. The concentration of Ba^{2+} ([Ba^{2+}]) (diamonds) that associates with accessible sulfonate groups in the active layer is also shown. Symbols represent experimental data. Error bars indicate standard deviation. The (red) continuous and (blue) dashed lines correspond to the average [R-SO$_3^-$] and [Ba^{2+}], respectively. (b) Accessibility ratio for Ba^{2+} ion (AR) in the SPES active layer. Circles are the values obtained by solving eq 5 using the average [R-SO$_3^-$] and experimental [Ba^{2+}] points from (a), and NN = 1.96 $\pm$ 0.05 from Table 1. Error bars indicate standard error. The dash-dot-dot line is the average AR value in the pH range tested.

for RO and NF membranes, respectively; the thinnest RO and NF active layers were 98 and 72 nm thick, respectively. Since water flux is inversely proportional to active layer thickness (*1, 2*), we hypothesize that one reason why fully aromatic polyamide RO active layers are not made thinner is because the relatively high standard deviation of the active layer thickness requires a minimum average thickness to attain salt rejection at RO levels.

In contrast, the SPES active layer of the NTR-7450 NF membrane was approximately 15% thicker than the thickest PA layer, and in particular about 40% thicker than that of the ESPA3 RO membrane; however, water permeability for the NTR-7450 membrane (2.1−6.4 $\times$ 10^{-11} m$\cdot$s$^{-1}\cdot$Pa^{-1} (*22*)) is higher than that for the ESPA3 membrane ($\approx$1.7 $\times$ 10^{-11} m$\cdot$s$^{-1}\cdot$Pa^{-1} (*23*)) indicating that active layer resistance to water transport per unit thickness of PA is higher than per unit thickness of SPES.

Ionization Behavior of Functional Groups. The concentration of ionized functional groups as a function of pH in the PA active layer of the LF10 RO membrane, as representative of PA membranes, and in the SPES active layer of the NTR-7450 NF membrane are shown in Figures 1a and 2a, respectively. The corresponding plots for the other PA membranes studied can be found in Figure S5 of SI. For PA active layers, the ionization of functional groups was modeled assuming acid−base equilibrium with the ion-probe solution as given by (*12*)

$$[\text{R-COO}^-] = C_{T,\text{R-COOH}} \sum_{i=1}^{n} \left(w_i \frac{10^{-\text{p}Ka,i}}{10^{-\text{pH}} + 10^{-\text{p}Ka,i}} \right) \quad (2)$$

and

$$[\text{R-NH}_3^+] = C_{T,\text{R-NH2}} \sum_{j=1}^{n} \left(w_j \frac{10^{-\text{pH}}}{10^{-\text{pH}} + 10^{-\text{p}Ka,j}} \right) \quad (3)$$

where $C_{T,\text{R-COOH}}$ and $C_{T,\text{R-NH2}}$ are the total concentrations of carboxylic (R-COOH/R-COO$^-$) and amine (R-NH$_3^+$/R-NH$_2$) groups, respectively, and w_i represents the fraction of functional groups having pK_a = p$K_{a,i}$ where $\sum_{i=1}^{n} w_i = 1$. Fitted values for all membranes are summarized in Table 1.

Consistent with our previous study of the FT30 RO membrane (*12*), two pK_a values were needed to describe the ionization behavior of carboxylic groups in PA active layers

(i.e., $n = 2$ in eq 2). The pK_a of carboxylic groups is a function of different factors that affect the stability of the conjugate base R-COO$^-$ (*24*) including, among others, the dielectric constant of the microenvironment surrounding the carboxylic groups (*24, 25*). Accordingly, we hypothesize (*12*) that the bimodal pK_a distribution of carboxylic groups in PA active layers is in part due to the bimodal pore size distribution reported for PA active layers (*3, 10, 26*); the size of the nanopores where water is contained affects the dielectric constant of water (*27*) which, in turn, affects the pK_a of carboxylic groups (*25*).

The ESPA3 RO membrane, however, had a pK_a distribution heavily biased toward one value ($w_2 = 0.92 \pm 0.07$), and a fitted dominant p$K_a = 5.86 \pm 0.10$ between the p$K_{a,1}$ and p$K_{a,2}$ of the other PA membranes. Consistent with the discussion above on the relation between pore size, water dielectric constant, and pK_a values, the dominant intermediate pK_a value of the ESPA3 RO membrane is likely indicative of a dominant intermediate pore size. This possibility is supported by the findings of Kim et al. (*3*) who showed that the use of additives such as dimethyl sulfoxide (DMSO) during the PA polymerization reaction results in pore size distributions biased toward a dominant size that is intermediate between the two sizes produced in the absence of DMSO, and by the reported (*3, 13*) use of additives such as DMSO in the production of high-flux RO membranes.

Table 1 shows that while the ESPA3 RO membrane had the highest $C_{T,\text{R-COOH}} = 0.64$ M, and the lowest p$K_{a,1} = 3.91$, p$K_{a,2} = 5.86$, and fraction $w_1 = 0.08 \pm 0.07$, the NF90 NF membrane had the lowest $C_{T,\text{R-COOH}} = 0.24$ M, and the highest p$K_{a,1} = 5.72$, p$K_{a,2} = 9.87$, and fraction $w_1 = 0.60 \pm 0.07$. The other four PA membranes had similar $C_{T,\text{R-COOH}}$ (0.50−0.54 M), p$K_{a,1}$ (5.23−5.42), and p$K_{a,2}$ (8.46−9.03), and w_1 fractions in the 0.22−0.49 range. The ESPA3 RO membrane reached 94% ionization by pH = 7, the NF90 NF membrane had a relatively stable charge density of ≈0.14 M in the pH range 7.0−9.0, and the other four PA membranes underwent a relatively steady increase in charge across the entire pH range. Accordingly, for the fully aromatic polyamide RO/NF membranes of our study, we found that (i) the total concentrations of carboxylic groups were in the 0.45 ± 0.25 M range; (ii) while the highest and lowest $C_{T,\text{R-COOH}}$ were obtained for RO and NF membranes, respectively, some RO and NF membranes had almost identical $C_{T,\text{R-COOH}}$; (iii) membranes with similar $C_{T,\text{R-COOH}}$ had relatively different ionization behaviors as a result of their varying pK_a and w_1 values; and (iv) the membranes with the highest and lowest $C_{T,\text{R-COOH}}$ also had the lowest and highest, respectively, p$K_{a,1}$, p$K_{a,2}$, and w_1 values.

For the case of amine groups (R-NH$_3^+$/R-NH$_2$), one pK_a sufficed to describe their ionization behavior. Table 1 shows that p$K_{a,\text{R-NH3+}}$ values were in the 3.63−4.62 range, and that $C_{T,\text{R-NH2}}$ values were in the 0.01−0.08 M range with $C_{T,\text{R-NH2}}$: $C_{T,\text{R-COOH}} \leq 0.08$ except for the NF90 NF membrane (0.33). The relatively low $C_{T,\text{R-NH2}}$ and pK_a for amine groups made the concentration of positive charges negligible (≤0.005 M) in the pH range of interest for water treatment (pH ≈ 6−10). While the highest $C_{T,\text{R-NH2}}$ (0.08 M) occurred in an NF membrane (NF90), the second highest (0.04 M) occurred in an RO membrane (FT30), thus indicating that there is no correlation between the concentration of amine groups and membrane designation (i.e., RO or NF). We obtained the isoelectric point in PA active layers as the intersection of [R-COO$^-$] and [WO_4^{2-}] curves in Figures 1a and S5. All isoelectric points fell in the pH ≈ 3−5 range consistent with the values reported in the literature from zeta potential analyses (*4, 21, 28*).

RBS characterization of the SPES active layer of the NTR-7450 NF membrane (see Figure 2a) revealed that the concentration of sulfonate groups was 1.67 M = 1.22 meq/g, consistent with the range of ion exchange capacities (1.0−1.6 meq/g) reported (*29*) for SPES copolymers with compositions similar to that of the active layer of the NTR-7450 membrane. In contrast to carboxylic groups in PA layers, sulfonate groups remained ionized in the pH range investigated (5.31−8.75), consistent with the relatively low p$K_a < 4$ of sulfonic groups (*30*). The concentration of sulfonate groups in the SPES active layer of the NTR-7450 NF membrane was 2.6 times higher than the highest $C_{T,\text{R-COOH}}$ (0.64 M) measured in PA active layers.

Degree of Polymer Cross-linking (DPC). We used the RBS data to calculate the degree of polymer cross-linking (DPC) in PA active layers using the expression (*12*)

$$\text{DPC} = \frac{\text{Amide links}}{\text{Potential amide links}} = \frac{\text{N} - \text{AG}}{\text{N} + \text{CG}} \qquad (4)$$

where DPC is the ratio between the measured concentration of amide links and the concentration of amide links in an equivalent fully cross-linked active layer, and N, AG, and CG are the concentrations in the active layer of nitrogen, amine groups, and carboxylic groups, respectively. Average DPC values were 94−95% and 95−97% for RO and NF membranes, respectively (Table 1). We also characterized the degree of cross-linking by calculating *n*, *x*, and *y* fractions of polymer repeating units in the PA structure that were fully cross-linked $(C_{36}H_{24}N_6O_6)_n$, contained a carboxylic group $(C_{36}H_{25}N_6O_7)_x$, and contained an amine group $(C_{36}H_{25}N_6O_6)_y$, respectively (*12*). We used the relations $x + y = 6 \times (\text{CG} + \text{AG})/\text{N}$, $x/y = \text{CG}/\text{AG}$, and $n + x + y = 1$ (*12*). The resulting *n* ranges for RO and NF membranes were 59−66% and 68−84%, respectively. Whereas both DPC and *n* values are equally reliable (i.e., both are calculated based on N, AG, and CG), DPC values are significantly less sensitive than *n* values to changes in N, AG, or CG; relatively small differences between degrees of cross-linking as quantified by the DPC are amplified when a polymer repeating unit structure is assumed as expressed by *n* values. As shown in Table 1, the difference in degree of cross-linking between the RO and NF membranes studied is not significant. Therefore DPC might be more intuitive than *n* as an indicator of relative differences in degrees of cross-linking.

Stoichiometry of Association between Negative Functional Groups and Ba^{2+}. Figure 3a shows the stoichiometry of association between R-COO$^-$ groups and Ba^{2+} ions in the PA active layers studied. The *y*-axis is the concentration of R-COO$^-$ groups neutralized by Ba^{2+}, and the *x*-axis is the concentration of Ba^{2+} ions neutralizing those sites. Accordingly, the average number of R-COO$^-$ groups neutralized per barium ion (Ba^{2+}) (*14*) is given by NN = *y*/*x* for any given (*x*,*y*) point. Figure 3b presents the calculated NN values as a function of the concentration of R-COO$^-$ groups neutralized by Ba^{2+} (i.e., the *x*-axis in Figure 3b is the same *y*-axis in Figure 3a).

In a previous study (*14*), we modeled the data for the FT30 RO membrane in Figure 3a based on a single parameter *a* such that $\Delta y/\Delta x = 1 \rightarrow y = x$ for $x \leq a$, and $\Delta y/\Delta x = 2 \rightarrow y = 2x - a$ for $x > a$. Accordingly, the *a* parameter represented the concentration of neutralized R-COO$^-$ groups at which the stoichiometry of association between the additional R-COO$^-$ sites (Δy) that ionized as pH increased and the Ba^{2+} ions (Δx) that neutralized them changed from 1:1 to 2:1. In other words, *a* represents the concentration of neutralized R-COO$^-$ groups at which the average distance between them becomes so small that some Ba^{2+} ions neutralize two R-COO$^-$ groups simultaneously; larger *a* values therefore indicate larger average distances between ionizable functional groups. We used the same model to fit the data for the other PA membranes, and obtained the corresponding *a* values and fitted lines shown in Table 1 and Figure 3a, respectively. Corresponding NN curves were plotted in Figure 3b. As

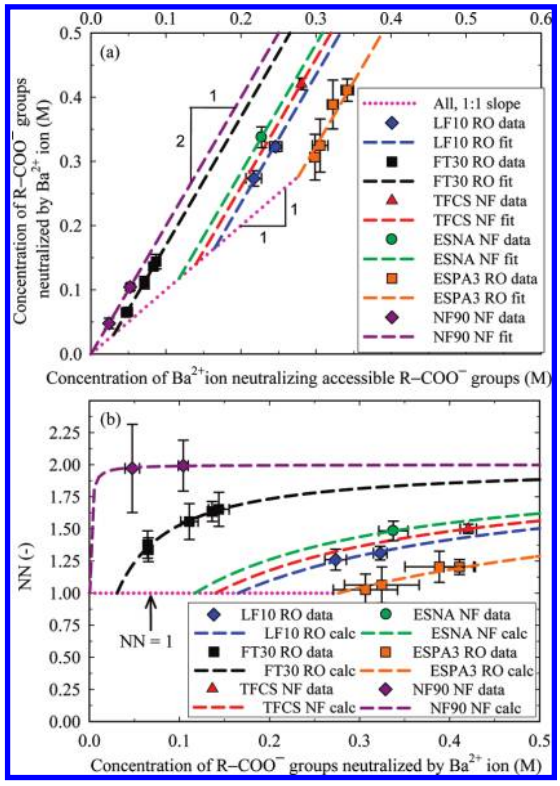

FIGURE 3. Stoichiometry of association between R-COO$^-$ groups neutralized by Ba^{2+} in the polyamide (PA) active layers of the membranes studied and the Ba^{2+} ions neutralizing them. (a) Limiting one-to-one (pink dotted line) and two-to-one (color dashed lines) correspondence between neutralized R-COO$^-$ groups and Ba^{2+} ion. Symbols are experimental data obtained from Ag^+−Ba^{2+} ion-displacement tests. The coordinates $(x,y) = (\alpha,\alpha)$ of the intersection of the 2:1 line of any membrane with the 1:1 line correspond to the value of the α parameter in Table 1 and eq 6. The neutralization number for Ba^{2+} ion (NN) for any given (x,y) point is calculated as its corresponding y/x ratio. (b) NN as a function of the concentration of R-COO$^-$ sites neutralized by Ba^{2+} ion in the PA active layers of the membranes studied. Symbols and lines are the NN values calculated from their corresponding plots in (a). Error bars indicate standard error.

depicted in the figures, fitted lines described well experimental data sets with multiple data points, thus supporting the validity of the model.

Figure 3 and Table 1 show that the a parameter was different for each membrane. Since a larger a indicates a larger average distance between ionized functional groups and $a_{Max} = a_{ESPA3\ RO} > a_{LF10\ RO} > a_{TFC\text{-}S\ NF} > a_{ESNA\ NF} > a_{FT30\ RO} > a_{NF90\ NF} = a_{Min}$, then the spatial distribution of carboxylic groups is different in each PA active layer studied. ESPA3 RO and NF90 NF have the most and the least, respectively, homogeneously distributed carboxylic groups in their active layers. Additionally, since RO membranes have both the largest and the second-lowest a values, there is no correlation between the a parameter and membrane designation as RO or NF.

We also performed an Ag^+−Ba^{2+} displacement test at pH = 5.96 with the NTR-7450 NF membrane to study the stoichiometry of association between its R-SO_3^- groups and Ba^{2+} ions, and found that NN = 1.96 ± 0.05. Since the concentration of R-SO_3^- groups in NTR-7450 as a function of pH is constant, then NN ≈ 2.0 at any pH.

Accessibility of Ba^{2+} Ion to Negative Functional Groups. In a previous study (*14*), we demonstrated that the concentration of barium ion ([Ba^{2+}]) that associated with accessible carboxylic groups in the PA active layer of the FT30 RO membrane was given by

$$[Ba^{2+}] = \frac{AR \times [R\text{-}COO^-]}{NN} \quad (5)$$

where the accessibility ratio AR is defined as the fraction of R-COO$^-$ groups accessible to Ba^{2+} ions. We also showed that NN was given by

$$NN = 2 \times \left(\frac{AR \times [R\text{-}COO^-]}{AR \times [R\text{-}COO^-] + a} \right) \quad (6)$$

for AR × [R-COO$^-$] > a, and NN = 1 for AR × [R-COO$^-$] ≤ a. Accordingly, in this study, we used eqs 5 and 6, the experimental ion-probing/RBS data for [R-COO$^-$] and [Ba^{2+}] as a function of pH, and the a parameter values obtained in the previous section, to calculate AR as a function of pH. The [Ba^{2+}] data and calculated AR values are presented in Figure 1 for LF10 RO and in Figure S5 of SI for all other membranes with PA active layers. The results show that, consistent with our previous findings for FT30 RO (*14*), AR was approximately constant as a function of pH except at the lowest pH ≈ 3.5 tested at which AR = 1. Average AR values were in the 0.40−0.81 range (see Table 1). The only membrane that deviated significantly from a constant AR across the entire pH range was NF90 NF for which AR varied from 0.45 ± 0.04 at pH = 3.5−6.6 to 0.69 ± 0.05 at pH = 7.5−10.4; however, an AR = 0.58 ± 0.03 satisfactorily described the average steric effects experienced by Ba^{2+} ion.

The average AR and a values of each membrane were used to calculate [Ba^{2+}] as a function of pH (see Figure 1a and Figure S5 of SI) using eqs 5 and 6. As observed in the figures, the calculated [Ba^{2+}] matches well the experimental data, thus indicating that for any given PA active layer, the two constant parameters AR and a describing the accessibility and stoichiometry of association, respectively, of carboxylic groups suffice to describe adequately the difference between [R-COO$^-$] and [Ba^{2+}] as a function of pH. Since for a given active layer, carboxylic groups likely have different pK_a values in pores of different sizes (see discussion above and in ref *14*), constant AR values for the entire pH range investigated are consistent with what we previously proposed for the FT30 RO membrane (*14*), i.e., that pores of different sizes in PA active layers are interconnected thus forming a network of pores that makes carboxylic groups equally accessible (or inaccessible) regardless of the size of the pore where they are located.

For the case of the SPES active layer of the NTR-7450 NF membrane, Figure 2a shows that [Ba^{2+}] = 0.81 ± 0.02 M was approximately constant in the entire pH range studied (3.38−10.15). Using eq 5 and NN = 1.96 ± 0.05 (see previous section), we calculated AR as a function of pH and plotted the results in Figure 2b. The results show that AR = 0.95 ± 0.01 which indicates that Ba^{2+} has access to ≈100% of the R-SO_3^- groups in the SPES active layer. Accordingly, the steric effects experienced by Ba^{2+} and other solutes of equal or greater size in fully aromatic PA active layers are greater than in the SPES active layer of the NTR-7450 NF membrane.

Acknowledgments

RBS analyses were carried out in the Center for Microanalysis of Materials, University of Illinois at Urbana−Champaign, partially supported by the U.S. Department of Energy under grants DE-FG02-07ER46453 and DE-FG02-07ER46471. We acknowledge Doug Jeffers for assistance in RBS analyses, Gorie Ster and Jeanne Luh for helpful discussions, and the companies Nitto Denko, Hydranautics, and Koch Membrane Systems for providing membrane materials and related information. This work was supported by the National Science

Foundation Environmental Engineering and Technology program under agreement BES-0332217, and the Water-CAMPWS, a Science and Technology Center of Advanced Materials for the Purification of Water with Systems under agreement CTS-0120978. The opinions in this paper do not necessarily reflect those of the sponsor.

Supporting Information Available

Figure S1 (Attenuated total reflectance Fourier transform infrared (ATR-FTIR) spectrometry analyses of membranes with polyamide (PA) active layers); Figure S2 (Rutherford backscattering spectrometry (RBS) spectrum of a sample of LF10 RO membrane probed with Ag^+ at pH = 9.85); Figure S3 (Repeating units in the polymer structure of the sulfonated polyethersulfone (SPES) active layer of the NTR-7450 NF membrane); Figure S4 (RBS spectra and corresponding simulations for (a) FT30 RO (see note *a* in Table 1), (b) LF10 RO, (c) ESPA3 RO, (d) TFC-S NF, (e) ESNA NF, (f) NF90 NF and (g) NTR-7450 NF membranes); Figure S5 (Concentration of ionizable functional groups, concentration of Ba^{2+} ion that associates with accessible R-COO^- groups, and accessibility ratio (AR) for Ba^{2+} ion as a function of pH in the active layers of (a) FT30 RO (see note *a* in Table 1), (b) ESPA3 RO, (c) TFC-S NF, (d) ESNA NF, and (e) NF90 NF membranes). This information is available free of charge via the Internet at http://pubs.acs.org.

Literature Cited

(1) Petersen, R. J. Composite reverse osmosis and nanofiltration membranes. *J. Membr. Sci.* **1993**, *83*, 81–150.
(2) Wijmans, J. G.; Baker, R. W. The solution-diffusion model: a review. *J. Membr. Sci.* **1995**, *107*, 1–21.
(3) Kim, S. H.; Kwak, S.-Y.; Suzuki, T. Positron annihilation spectroscopic evidence to demonstrate the flux-enhancement mechanism in morphology-controlled thin-film-composite (TFC) membrane. *Environ. Sci. Technol.* **2005**, *39*, 1764–1770.
(4) Childress, A. E.; Elimelech, M. Relating nanofiltration membrane performance to membrane charge (electrokinetic) characteristics. *Environ. Sci. Technol.* **2000**, *34*, 3710–3716.
(5) Helfferich, F. *Ion Exchange*; McGraw-Hill: New York, 1962.
(6) Bartels, C. R. A surface science investigation of composite membranes. *J. Membr. Sci.* **1989**, *45*, 225–245.
(7) Brant, J. A.; Johnson, K. M.; Childress, A. E. Characterizing NF and RO membrane surface heterogeneity using chemical force microscopy. *Colloids Surf., A* **2006**, *280*, 45–57.
(8) Elimelech, M.; Zhu, X.; Childress, A. E.; Hong, S. Role of membrane surface morphology in colloidal fouling of cellulose acetate and composite aromatic polyamide reverse osmosis membranes. *J. Membr. Sci.* **1997**, *127*, 101–109.
(9) Cahill, D. G.; Freger, V.; Kwak, S.-Y. Microscopy and microanalysis of reverse osmosis and nanofiltration membranes. *MRS Bull.* **2008**, *33*, 27–32.
(10) De Baerdemaeker, J.; Boussu, K.; Djourelov, N.; Van der Bruggen, B.; Dauwe, C.; Weber, M.; Lynn, K. G. Investigation of nanopores in nanofiltration membranes using slow positron beam techniques. *Phys. Status Solidi* **2007**, *4*, 3804–3809.
(11) Mi, B.; Coronell, O.; Mariñas, B. J.; Watanabe, F.; Cahill, D. G.; Petrov, I. Physico-chemical characterization of NF/RO membrane active layers by Rutherford backscattering spectrometry. *J. Membr. Sci.* **2006**, *282*, 71–81.
(12) Coronell, O.; Mariñas, B. J.; Zhang, X.; Cahill, D. G. Quantification of functional groups and modeling of their ionization behavior in the active layer of FT30 reverse osmosis membrane. *Environ. Sci. Technol.* **2008**, *42*, 5260–5266.
(13) Freger, V. Nanoscale heterogeneity of polyamide membranes formed by interfacial polymerization. *Langmuir* **2003**, *19*, 4791–4797.
(14) Coronell, O.; Mariñas, B. J.; Cahill, D. G. Accessibility and ion exchange stoichiometry of ionized carboxylic groups in the active layer of FT30 reverse osmosis membrane. *Environ. Sci. Technol.* **2009**, *43*, 5042–5048.
(15) Pourbaix, M. *Atlas of Electrochemical Equilibria in Aqueous Solutions*; 1st English ed.; Pergamon Press: Great Britain, 1966.
(16) Mi, B.; Mariñas, B. J.; Cahill, D. G. RBS characterization of arsenic (III) partitioning from aqueous phase into the active layers of thin-film composite NF/RO membranes. *Environ. Sci. Technol.* **2007**, *41*, 3290–3295.
(17) Mi, B.; Cahill, D. G.; Mariñas, B. J. Physico-chemical integrity of nanofiltration/reverse osmosis membranes during characterization by Rutherford backscattering spectrometry. *J. Membr. Sci.* **2007**, *291*, 77–85.
(18) Mayer, M.; Duggan, J. L.; Morgan, I. L. SIMNRA, a simulation program for the analysis of NRA, RBS and ERDA. In *Proceedings of the 15th International Conference on the Application of Accelerators in Research and Industry*, 1998, Denton, TX.
(19) Hachisuka, H.; Ikeda, K. Reverse osmosis composite membrane and reverse osmosis treatment method for water using the same. US Patent 6,413,425 B1, 2002.
(20) Tang, C. Y.; Kwon, Y.-N.; Leckie, J. O. Effect of membrane chemistry and coating layer on physiochemical properties of thin film composite polyamide RO and NF membranes I. FTIR and XPS characterization of polyamide and coating layer chemistry. *Desalination* **2009**, *242*, 149–167.
(21) Tang, C. Y.; Kwon, Y.-N.; Leckie, J. O. Probing the nano- and micro-scales of reverse osmosis membranes-A comprehensive characterization of physiochemical properties of uncoated and coated membranes by XPS, TEM, ATR-FTIR, and streaming potential measurements. *J. Membr. Sci.* **2007**, *287*, 146–156.
(22) Bargeman, G.; Vollenbroek, J. M.; Straatsma, J.; Schroën, C. G. P. H.; Boom, R. M. Nanofiltration of multi-component feeds. Interactions between neutral and charged components and their effect on retention. *J. Membr. Sci.* **2005**, *247*, 11–20.
(23) Louie, J. S.; Pinnau, I.; Ciobanu, I.; Ishida, K. P.; Ng, A.; Reinhard, M. Effects of polyether-polyamide block copolymer coating on performance and fouling of reverse osmosis membranes. *J. Membr. Sci.* **2006**, *280*, 762–770.
(24) Jacobs, A. *Understanding Organic Reaction Mechanisms*; Cambridge University Press: Cambridge, United Kingdom, 1997.
(25) Bacarella, A. L.; Grunwald, E.; Marshall, H. P.; Lee Purlee, E. The potentiometric measurements of acid dissociation constants and *p*H in the system methanol-water. pK_A values for carboxylic acids and anilinium ions. *J. Org. Chem.* **1955**, *20*, 747–762.
(26) Harder, E.; Walters, D. E.; Bodnar, Y. D.; Faibish, R. S.; Roux, B. Molecular dynamics study of a polymeric reverse osmosis membrane. *J. Phys. Chem. B* **2009**, *113*, 10177–10182.
(27) Senapati, S.; Chandra, A. Dielectric constant of water confined in a nanocavity. *J. Phys. Chem. B* **2001**, *105*, 5106–5109.
(28) Childress, A. E.; Elimelech, M. Effect of solution chemistry on the surface charge of polymeric reverse osmosis and nanofiltration membranes. *J. Membr. Sci.* **1996**, *119*, 253–268.
(29) Ikeda, K.; Yamamoto, S.; Ito, H. Sulfonated polysulfone composite semipermeable membranes. European Patent EP 0 165 077 B2, 1998.
(30) Vaidya, B.; Soper, S. A.; McCarley, R. L. Surface modification and characterization of microfabricated poly(carbonate) devices: manipulation of electroosmotic flow. *Analyst* **2002**, *127*, 1289–1292.
(31) Zhang, X.; Cahill, D. G.; Coronell, O.; Mariñas, B. J. Absorption of water in the active layer of reverse osmosis membranes. *J. Membr. Sci.* **2009**, *331*, 143–151.
(32) Solvay Membranes: Product Information. Available at http://www.solvayadvancedpolymers.com/products/byproducttype/sulf/0,53267-2-0,00.htm (Accessed October 30, 2009).
(33) Van Krevelen, D. W. *Properties of Polymers*; 3rd Completely Revised ed.; Elsevier Publishing Company: New York, 1990.

ES100891R